Investigations of the Modified Navier-Stokes Equations in One Dimension

Master thesis in Applied and Computational Mathematics

Inga Sofie Sårheim

Department of Mathematics
University of Bergen
June 2, 2014

Acknowledgements

First of all, I would like to thank my supervisor Magnus Svärd for all help and support.

Secondly, I would like to thank my friends and fellow students for making my years at the university amazing and memorable.

Thanks to my boyfriend, my parents and my family for all their everlasting support and patience.

Inga Sofie, June 2014

Contents

Symbols

E	energy
F	entropy flux
Kn	Knudsen number
L	length scale of interest
M	Mach number
Q	numerical diffusion matrix
R	gas constant
T	temperature
U	entropy variable
c	speed of sound
c_p	specific heat capacity with constant pressure
c_v	specific heat capacity with constant volume
k	heat conductivity
m	momentum
p	pressure
t	time variable
$\mathbf{u}$	velocity vector
$\mathbf{u}_v$	volume velocity
u	velocity in 1D
u_t	partial derivative of u with respect to t
u_x	partial derivative of u with respect to x
x	1D space variable
Ω	fixed volume
α_v	volume diffusivity
β	energy approximation
γ	ratio of specific heats

δ	mass diffusion
λ	mean free path
μ	viscosity
ρ	density

Introduction

The Navier-Stokes equations are a set of equations which describes the motion of a fluid, and they are the most fundamental equations in fluid mechanics. They state that the fluid particle's change in momentum is the product of the change in pressure, and the dissipation of viscous forces. The viscous forces can be described as friction forces that have an effect on the fluid itself.

Even though the Navier-Stokes equations are assumed to be a correct model of how a fluid flow, it turns out that they are not completely accurate in all situations. This is evident when e.g. modeling a shock wave. In this thesis, an alternative model of the Navier-Stokes equations, the Brenner-Navier-Stokes equations, is presented for one spatial dimension. The modified equations adds an extra diffusion term to the Navier-Stokes system, which we consider to be mass diffusion. We investigate the possibility that the diffusion happening in a fluid depends on the density of the fluid in addition to the velocity. The mass diffusion has little or no effect in the cases where the Navier-Stokes equations work well. Brenner's model can be a more physically realistic model for fluid flow than the original Navier-Stokes equations.

The model will be tested with shock wave simulations in argon, done in Matlab, using a finite difference discretization. We will experiment with both entropy-stable and entropy-consistent schemes. The results will be analyzed, and compared to experimental results.

The results presented in this report has been bounded to a Mach 8 shock in argon, because of limited experimental results for comparison. Nevertheless,

we have done simulations with Mach 2-7 shocks, with similar results to those presented for the Mach 8 shock.

The thesis is organized as follows: **Chapter 1** gives the most basic definitions and presents an overview of the basic principles behind the Brenner-Navier-Stokes equations. **Chapter 2** gives the characteristics of the discretization and simulation. In **Chapter 3** the results for our simulation is presented, analyzed and compared to experimental results and **Chapter 4** gives concluding remarks and ideas for further work. The details about the Ismail and Roe's entropy-consistent Euler flux is given in **Appendix A**, and **Appendix B** gives the data values used in this thesis.

Chapter 1

Fluid Flow and the Navier-Stokes Equations

This chapter summarizes the basic definitions, and presents an overview of the basic principles behind the Brenner-Navier-Stokes equations. It is however assumed that the reader is familiar with the most used concepts of fluid mechanics. For a deeper review, see [11] and [12], which the introductory theory in Sections 1.1-1.3 has been the based on. The theory from Section 1.4 is based on [9] and [10], and Section 1.5 is based on [4] and [5]. Section 1.6 is based on [7], [8] and private conversation with Professor Magnus Svärd.

1.1 Conservation laws

Conservation laws describe how fluid properties, like mass, momentum and energy, is conserved within a closed system.

Conservation of mass is based on the observation that mass is never created nor destroyed, in Newtonian physics. If a specific collection of mass particles are tracked inside a fixed volume $\Omega(t)$ with the density $\rho(\mathbf{x}, t)$, the mass within will be conserved while the volume moves or deforms. Thus,

we have

$$\frac{\partial \rho}{\partial t} + \nabla \cdot (\rho \mathbf{u}) = 0, \tag{1.1}$$

which is the conservation of mass equation, often referred to as the continuity equation. The volume moves with the velocity $\mathbf{u}$.

The momentum-conservation equivalent of equation (1.1) is developed from Newton's second law. Similarly as for the continuity equation, the **conservation of momentum** equation becomes

$$\frac{\partial \rho \mathbf{u}}{\partial t} + \nabla \cdot ((\rho \mathbf{u})\mathbf{u}) + \nabla \cdot \mathbf{p} = \mathbf{g} + \nabla \frac{4}{3}\mu \nabla \mathbf{u}, \tag{1.2}$$

where $\mathbf{p}$ is the pressure, $\mathbf{g}$ is the volume forces working in Ω and $\mu > 0$ is the dynamic viscosity.

From the first law of thermodynamics, which states that energy cannot be created nor destroyed, only transformed into other forms, we get **conservation of energy** similar to mass and momentum

$$\frac{\partial E}{\partial t} + \nabla \cdot (E\mathbf{u}) + \nabla \cdot \mathbf{p} = \nabla(k \nabla T) - \nabla \cdot (u \cdot \frac{4}{3}\mu \nabla \mathbf{u}). \tag{1.3}$$

The total energy per unit mass is given as $E = \frac{1}{2}\rho u^2 + \frac{p}{\gamma - 1}$, where γ is the ratio of the specific heat capacities, T is the temperature and $k > 0$ is the heat conductivity.

The conservation laws are valid when the length scales used are much larger than the molecular distances. We measure this by using the Knudsen number

$$Kn = \lambda / L, \tag{1.4}$$

where λ is the average distance traveled by a particle, called the mean free path, and L is the length scale we use, e.g. the size of a shock. The validity is satisfied when $Kn << 1$.

1.2 The Navier-Stokes equations

We can unite the conservation laws in a system of equations on conservation form. For a Newtonian fluid in one dimension (1D) they constitute the 1D

Navier-Stokes equations

$$\mathcal{U}_t + f(\mathcal{U})_x = (f^{\mathrm{NS}})_x, \tag{1.5}$$

$$\mathcal{U} = [\rho, m, E]^T, \tag{1.6}$$

$$f(\mathcal{U}) = [m, \rho u^2 + p, (E + p)u]^T, \tag{1.7}$$

$$f^{\mathrm{NS}} = \left[0, \frac{4}{3}\mu u_x, \frac{4}{3}\mu u u_x + kT_x\right]^T, \tag{1.8}$$

where $\mathcal{U}$ represents the conserved quantity. The momentum is denoted as $m = \rho u$. The system is closed using the gas law $p = \rho RT$ where R is the gas constant.

1.3 Shock waves

When $0.01 \lesssim Kn < 1$ the use of the classical Navier-Stokes equations (1.5) is limited. A typical situation where this applies is when modeling a shock wave, because of the almost discontinuous conditions. Since the Navier-Stokes equations perform poorly at these Knudsen numbers, the shock structure problem is particularly interesting for testing an alternative models of the modified Navier-Stokes equations.

A shock wave is formed when the speed of a fluid changes more than the speed of sound in a medium. That is when the Mach number $M = \frac{u}{c} > 1$, where u is the speed of the disturbance and c the local speed of sound. For a shock with $Kn = 0.2 \sim 0.3$, this corresponds to a $M = 2$ or higher shock [8].

We use the *Rankine-Hugoniot relations* [12] to describe the relationship between the upstream (1) and the downstream (2) pressure, Mach number,

density and temperature of a shock

$$\frac{p_2}{p_1} = 1 + \frac{2\gamma}{\gamma+1}(M_1^2 - 1), \tag{1.9}$$

$$M_2^2 = \frac{(\gamma-1)M_1^2 + 2}{2\gamma M_1^2 + 1 - \gamma}, \tag{1.10}$$

$$\frac{\rho_2}{\rho_1} = \frac{u_1}{u_2} = \frac{(\gamma+1)M_1^2}{(\gamma-1)M_1^2 + 2}, \tag{1.11}$$

$$\frac{T_1}{T_2} = 1 + \frac{2(\gamma-1)}{(\gamma+1)^2}\frac{\gamma M_1^2 + 1}{M_1^2}(M_1^2 - 1). \tag{1.12}$$

1.4 Weak solutions

Conservation laws may produce discontinuous solutions, and at the moment the differential form of the equation breaks down, the solution is no longer valid. However, the discontinuous solutions may be accurate representatives of a natural phenomena. A *weak solution* can then be used to broaden our definition of a solution.

We let $\phi(t,x) \geq 0$ be a test function, and multiply our non-linear problem by ϕ and integrate in time and space. For the viscous conservation law, as the Navier-Stokes equations,

$$\begin{aligned} &\mathcal{U}_t + f(\mathcal{U})_x = (G(\mathcal{U})\mathcal{U}_x)_x, \\ &\mathcal{U}(x,0) = \mathcal{U}_0(x), \end{aligned}$$

where $G(\mathcal{U})$ represents the viscous term f^{NS}. The local integrable function $\mathcal{U}$ is defined as a weak solution if it satisfy the following integral identity for all $\phi \in C^\infty(\Omega \times \mathbb{R}_+)$

$$\int_{\mathbb{R}_+}\int_\Omega \mathcal{U}\phi_t + f(\mathcal{U})\phi_x dxdt + \int_{\mathbb{R}_+}\int_\Omega \mathcal{U}_0(x)\phi(x,0)dxdt = -\int_{\mathbb{R}_+}\int_\Omega \phi_x G\mathcal{U}_x dxdt. \tag{1.13}$$

An important observation is that a non-linear problem can be well defined even if $\mathcal{U}$ is neither differentiable nor continuous. However, a weak solution is not necessarily a unique solution, but since a strong solution imply a weak one, proving a weak solution exists is a good place to start.

It is not necessarily easy to prove the existence of a weak solution by using the definition above. However, it appears that computational mathematics can be of great assistance here. The *Lax-Wendroff theorem* [9] states that *if a conservative numerical scheme for a system of conservation laws converges, then it converges towards a weak solution.*

Note that the theorem states that *if* a scheme converges to a solution, then the solution is a weak solution of the original problem. It does not guarantee that it will converge, nor that the weak solution obtained will satisfy the entropy condition, which is discussed below.

1.5 Conservation of entropy

Entropy is a physical quantity which is conserved in smooth solutions, but increases (or decreases, depending on the sign convention) if shock waves appears. Numerical methods for conservation laws will usually indicate this, but correspondence will only be precise for certain methods. A method is said to be *entropy-conservative* if the local changes of entropy are exactly the same as the entropy conservation law predicts. It is said to be *entropy-stable* if it produces more entropy than an entropy-conservative scheme. If the amount of entropy produced is correct, we say that the scheme is *entropy-consistent.*

Using an entropy-conservative schemes means that we have a higher probability for calculating the physical correct solution. Since a weak solution is not unique, there may be several solutions that satisfy equation (1.13). If we have more than one solution, one might be more physically realistic then the other. We usually consider this our "real" solution. Using a entropy-stable or entropy-conservative scheme that converges, the solution may converge to a physically more realistic solution.

It has been shown by Tadmor [4, 5] that stationary shocks can be captured by solving the Navier-Stokes equations with an entropy conserving Euler flux and central differences for the dissipation.

Consider a steady, discrete representation of a 1D shock wave. We assume that it has been produced by some stable, consistent, conservative numerical

method, with boundary conditions at the in- and outflow derived from the Rankine-Hugoniot conditions. Whether the scheme makes an explicit reference to entropy, or not, there will be some entropy flux at the inflow and some at the outflow. The nature of the scheme guarantees that these fluxes are correct, because they can be derived from the conserved variables.

The entropy production inside the domain corresponds to the difference of the two entropy fluxes. It follows that the entropy production within the domain is correct under the stated assumptions, once a steady state has been reached. If no entropy is produced, the scheme could not be stable.

Compared to the physical conservation laws in one dimension

$$\partial_t \mathcal{U} + \partial_x f = 0,$$

the conservation law for entropy takes the form

$$\partial_t U + \partial_x F \leq 0.$$

U denotes an entropy and F an entropy flux. The equality holds in regions with smooth flow, and the inequality may hold if the flow contains discontinuities.

In the cases where entropy is produced, the physical mechanism responsible is not represented in the original conservation law. Typically this is a dissipative or dispersive process, which mathematically is represented with higher order derivatives multiplied with some parameter.

We will get back to how our entropy-stable and entropy-consistent schemes looks like in Section 2.1.

1.6 Brenner's modification to the Navier-Stokes equations

In the Navier-Stokes equations (1.5) it is assumed that ρ is in equilibrium, and therefore there is no diffusion related to it. H. Brenner questions if this is true when ρ_x is large, and published a paper about it in 2005 [8]. Several papers, as [1, 7, 8], have been published later where his model has been discussed.

Brenner suggested that the volume velocity $\mathbf{u}_v$ is generally different from the mass velocity $\mathbf{u}$ in the mass conservation equation (1.1). The two velocities are connected by a *diffusive volume flux density* $\mathbf{j}_v = \mathbf{u}_v - \mathbf{u}$. A constitutive model relates $\mathbf{j}_v$ to $\nabla\rho$ by

$$\mathbf{j}_v = \alpha_v \frac{1}{\rho} \nabla\rho, \tag{1.14}$$

where α_v is the *volume diffusivity*. From this Brenner derived his modifications to the Navier-Stokes equations. The governing transport equations of mass, momentum and energy remained unchanged, while the convective mass velocity is replaced with the volume velocity [1].

This makes the modified 1D Navier-Stokes equations look like

$$\mathcal{U}_t + f(\mathcal{U})_x = (f^{\mathrm{NS}})_x + (f^{\mathrm{mod}})_x, \tag{1.15}$$

$$f^{\mathrm{NS}} = \left[0, \frac{4}{3}\mu u_x, \frac{4}{3}\mu u u_x + kT_x\right]^T, \tag{1.16}$$

$$f^{\mathrm{mod}} = \left[\alpha_v \rho_x, \alpha_v u \rho_x, \alpha_v E \rho_x\right]^T. \tag{1.17}$$

f^{NS} represents the viscous term of the Navier-Stokes equations, and f^{mod} the mass diffusion.

For fluids consisting of only one component going through a heat transfer, Brenner related α_v directly to the thermal diffusivity $\alpha_v = \alpha = k/\rho c_p$ [8], where c_p is the specific heat capacity under constant pressure.

Brenner's modified Navier-Stokes model has been examined and tested with generally promising results.

Independent of Brenner, Svärd[1] has developed an equivalent modification to the Navier-Stokes equations. The idea is that in addition to the known diffusion coefficients in the Navier-Stokes equations, there are several mass diffusion terms which also adds perturbations to the diffusion of the fluid. He wished to perturb the system (1.5) by adding mass diffusion in a way that keeps the entropy inequality of the Navier-Stokes equations, where the amount of entropy produced corresponds with what the entropy conservation law predicts.

[1] Unpublished

Svärd's perturbed system is equivalent to the Brenner-Navier-Stokes system

$$\mathcal{U}_t + f(\mathcal{U})_x = (f^{\mathrm{NS}})_x + (f^{\mathrm{mod}})_x, \tag{1.18}$$

$$f^{\mathrm{NS}} = \left[0, \frac{4}{3}\mu u_x, \frac{4}{3}\mu u u_x + kT_x\right]^T, \tag{1.19}$$

$$f^{\mathrm{mod}} = \left[\delta\rho_x, \delta u\rho_x, \delta\beta\rho_x\right]^T. \tag{1.20}$$

The diffusion coefficient $\delta > 0$ is identical to α_v in equation (1.18), and β is an approximation of the energy E. This system is entropy consistent in the sense that it is by construction symmetrizable by the physical entropy, just like the standard Navier-Stokes system. Up to a scaling, this is the only entropy consistent way to add mass diffusion.

There are several different ways to model the diffusion coefficients. In [8], Greenshields and Reese assumes that the dynamic viscosity obey a power law $\mu = AT^s$, where $s \in [0.5, 1]$. However, we will assume that it takes the similar form[2]

$$\mu(T) = \mu_0 + \mu_1\sqrt{T}. \tag{1.21}$$

μ_0 and μ_1 are constant coefficients determined from experiments and physical considerations, and $\mu(T) > 0$ in the applicable temperature interval.

Similarly

$$k = k_0 + k_1 T^2, \tag{1.22}$$

where the positive constants k_0 and k_1 are to be determined from experiments and physical considerations.

The viscosity and the thermal conductivity are both macroscopic representations of microscopic random movements, and they are not independent. The preferred relationship between μ and k seems to be $\mu = \frac{3k}{4c_p}$ for monoatomic ideal gases. This would imply that $k \sim \sqrt{T}$, just as μ. For the theoretical reasons mentioned above, we will however continue to use the relationship (1.22).

[2]This form is chosen to try to prove that the scheme approximates a weak solution.

In [8], the value of δ is discussed, and $\delta = \delta_0 = constant$ seems to be a more accurate choice than Brenner's original suggestion, where $\delta \sim 1/\rho$. We will use $\delta = \delta_0$.

We will return to how the diffusion coefficients are chosen in Section 2.2.

Chapter 2

Numerical Discretization of the Brenner-Navier-Stokes System

This chapter explains the implementations of the algorithms for the Brenner-Navier-Stokes simulation of a shock wave using theory from [5] and [14].

We discretize the domain Ω_N with $N+2$ grid points $x_i = ih,\ i = 0 \dots N+1$. At each grid point we associate a numerical solution variable, e.g. $\rho(x_i, t) = \rho_i$ at x_i. We use similar notation for all variables.

We use the time constant boundary conditions $\rho_0^{t_0} = \rho_0^{T_{\text{end}}}$ and $\rho_{N+1}^{t_0} = \rho_{N+1}^{T_{\text{end}}}$, where the superscript represents the time discretization, $t \in [t_0, T_{\text{end}}]$.

The Rankine-Hugoniot relations, (1.9)-(1.12), has been used as boundary conditions between the upstream and the downstream of the shock.

2.1 Entropy-consistent schemes

For the entropy production to be equivalent to what it is in a shock wave, we have two requirements. First we require conservation and stability of the scheme, such that the rise of entropy across the shock is correct. Secondly,

we need to make sure that the entropy contained within the shock is neither too great nor too small. This would result in the shock being smeared out or oscillatory, respectively.

We add a perturbation $\epsilon\mathcal{U}_{xx}$ in the form of a viscous term to the conservation law, such that $\mathcal{U}_t + f_x = \epsilon\mathcal{U}_{xx}$. If the limiting solution exists as $\epsilon \to 0$, the solution will satisfy the entropy inequality $U_t + F_x \leq 0$, and consequently we obtain an estimate for $U(\mathcal{U})_t \leq 0$.

The idea of entropy stable schemes is to approximate the non-diffusive conservation law and add a numerical diffusion, corresponding to the $\epsilon\mathcal{U}_{xx}$-term, which vanishes as $h \to 0$. The following semi-discrete form is analyzed in [4]

$$(\mathcal{U}_i)_t + \frac{f_{i+1/2} - f_{i-1/2}}{h} = 0. \tag{2.1}$$

Here $f_{i+1/2} = \frac{f(\mathcal{U}_i)+f(\mathcal{U}_{i+1})}{2} - \frac{Q_{i+1/2}}{2}(\mathcal{U}_{i-1} - \mathcal{U}_i)$ is the Euler flux, with the numerical diffusion matrix $Q_{i+1/2}$.

One of the forms of diffusion we will use is the local LaxFriedrichs diffusion, where $Q_{i+1/2} = \lambda_{i+1/2}I$. Here I is the 3×3 identity matrix and $\lambda_{i+1/2}$ is the maximum of the eigenvalues of the derivative flux $f_{\mathcal{U}}$ at x_i and x_{i+1}, e.i. $\max(|u_i| + c_i, |u_{i+1}| + c_{i+1})$. Here u_i and c_i is the discrete velocity and speed of sound.

For the m^{th} component $\mathcal{U}_i^m$ of $\mathcal{U}_i$, the scheme can be written

$$(\mathcal{U}_i^m)_t + \frac{f_{i+1}^m - f_{i-1}^m}{2h} = \frac{h}{2}D_-\lambda_{i+1/2}D_+\mathcal{U}_i, \tag{2.2}$$

where D_+ and D_- are the forward and backward derivatives,

$$D_+\rho_i = \frac{\rho_{i+1} - \rho_i}{h}, \tag{2.3}$$

$$D_-\rho_i = \frac{\rho_i - \rho_{i-1}}{h}. \tag{2.4}$$

The Lax-Friedrichs flux (2.2) leads to first order accuracy for smooth solutions, and is known to be very diffusive. For problems with very strong shocks, diffusion may be necessary, but the Lax-Friedrichs scheme may be too diffusive to give a physical realistic solution.

Ismail and Roe [5] developed a stable entropy-consistent flux with no artificial diffusion in the entropy. The entropy of the system will never decrease, except at the boundaries, and the total diffusion comes only from physical diffusion. The details of the flux is given in Appendix A.

Both Lax-Friedrichs and Ismail-Roe fluxes will be used for the simulations and compared with experimental data.

2.2 Numerical approximations

We have considered the following scheme for equation (1.18), (1.21) and (1.22).

$$(\rho_i)_t + \frac{f^1_{i+1/2} - f^1_{i-1/2}}{h} = D_- f^{\text{mod},1}_{i+1/2}, \tag{2.5}$$

$$((\rho u)_i)_t + \frac{f^2_{i+1/2} - f^2_{i-1/2}}{h} = D_- f^{\text{mod},2}_{i+1/2} + D_- f^{\text{NS},2}_{i+1/2}, \tag{2.6}$$

$$(E_i)_t + \frac{f^3_{i+1/2} - f^3_{i-1/2}}{h} = D_- f^{\text{mod},3}_{i+1/2} + D_- f^{\text{NS},3}_{i+1/2}, \tag{2.7}$$

where $f^j_{i+1/2}, \quad j = 1, 2, 3$ is the entropy-stable Euler flux.

The Lax-Friedrichs flux is given as

$$\begin{aligned} f^j_{i+1/2} &= \frac{f^j_{i+1} + f^j_i}{2} - \frac{\lambda_{i+1/2}}{2}(u^j_{i+1} - u^j_i), \\ [f^1_i, f^2_i, f^3_i]^T &= [(\rho u)_i, (\rho u^2 + p)_i, (u(E+p))_i]^T, \\ [\mathcal{U}^1_i, \mathcal{U}^2_i, \mathcal{U}^3_i]^T &= [\rho_i, (\rho u)_i, E_i]^T. \end{aligned} \tag{2.8}$$

The Ismail-Roe flux discretization is given in Appendix A.

The viscous fluxes are approximated by

$$\begin{bmatrix} f^{\mathrm{mod},1} \\ f^{\mathrm{mod},2} \\ f^{\mathrm{mod},3} \end{bmatrix}_{i+1/2} = \delta \begin{bmatrix} D_+\rho_i \\ \hat{u}_{i+1/2} D_+\rho_i \\ \hat{\beta}_{i+1/2} D_+\rho_i \end{bmatrix},$$

$$\begin{bmatrix} f^{\mathrm{NS},1} \\ f^{\mathrm{NS},2} \\ f^{\mathrm{NS},3} \end{bmatrix}_{i+1/2} = \begin{bmatrix} 0 \\ \frac{4}{3}\mu_{i+1/2} D_+ u_i \\ \frac{4}{3}\mu_{i+1/2}\hat{u}_{i+1/2} D_+ u_i + k_{i+1/2} D_+ T_i \end{bmatrix},$$

where

$$\begin{aligned} \hat{u}_{i+1/2} &= \frac{u_{i+1} + u_i}{2}, \\ \hat{\beta}_{i+1/2} &= \frac{u_{i+1}u_i}{2} + c_v \frac{\log(T_{i+1}/T_i)}{\frac{T_{i+1}-T_i}{T_{i+1}T_i}} && \text{if } T_i \neq T_{i+1}, \\ \hat{\beta}_{i+1/2} &= \frac{u_{i+1}u_i}{2} + c_v T_i && \text{if } T_i = T_{i+1}. \end{aligned}$$

The diffusion coefficients defined in equation (1.21) and (1.22) are approximated as

$$\delta = \delta_0, \tag{2.9}$$

$$\mu_i = \mu_0 + \mu_1 \sqrt{\tilde{T}_i}, \tag{2.10}$$

$$k_i = k_0 + k_1 T_i T_{i+1}. \tag{2.11}$$

$\tilde{T}_{i+1/2}$ is the inverse harmonic mean value

$$\tilde{T}^{-1}_{i+1/2} = \frac{1}{2}\left(\frac{1}{T_{i+1}} + \frac{1}{T_i}\right) = \frac{1}{2}\frac{T_{i+1} + T_i}{T_{i+1}T_i}.$$

2.3 Time discretization

Time-dependent partial differential equations are solved in several stages. We usually start by discretization of the spatial variables, to obtain a system of ordinary differential equations in the time variable. The semi-discrete

system can then be discretized by a stable solver. For problems with discontinuous solutions we can use a high-order strong stability-preserving time discretization method. We will use the three-stage third-order Runge-Kutta method in our simulations, because of its time-stability, simplicity and efficiency. For a deeper review of this discretization method, we refer to [3, 14].

Consider the semi-discrete system

$$\mathscr{U}_t = \mathbf{F}(\mathscr{U}(t)), \tag{2.12}$$

where $\mathscr{U}$ is a vector with elements containing all the spatial differential equations, and $\mathbf{F}$ is a vector valued function of $\mathscr{U}$. The three-stage third-order Runge-Kutta method will then be

$$\mathscr{U}^{m+1} = \mathscr{U}^m - \frac{\kappa}{9}\left(2K_1 + 3K_2 + 4K_3\right), \tag{2.13}$$

where

$$\begin{cases} K_1 &= \mathbf{F}(\mathscr{U}(t^m)) \\ K_2 &= \mathbf{F}\left(\mathscr{U}(t^m) + \kappa\frac{K_1}{2}\right) \\ K_3 &= \mathbf{F}\left(\mathscr{U}(t^m) + \kappa\frac{3K_2}{4}\right), \end{cases} \tag{2.14}$$

and κ is the time-dependent step size.

Chapter 3

Numerical Results

The investigation of the Brenner-Navier-Stokes equations, which has been the main task in this thesis, we have chosen to do by computing shock wave simulations with different diffusion models. The diffusion models used were limited to constant and variable (classical) diffusion and heat conductivity parameters, with and without mass diffusion (e.g. classical Navier-Stokes). The parameters have been based on physical measurements. The different diffusion models have been used to display the large variations small changes make, and show how Brenner's model solves the shock wave problem compared to the Navier-Stokes equations. Since our experimental data is of the density profile, we mainly focus on this in our results. The experimental data used for comparison were found in [2]. The different diffusion coefficients used can be found in Appendix B, together with the thermodynamic properties from [6], and the experimental values.

The Euler flux in the Naver-Stokes (and Brenner-Navier-Stokes) equations has been calculated in two different ways in the simulations presented. First, we used the Lax-Friedrichs method, which gives an entropy-stable scheme. In addition we used the entropy-consistent scheme, developed by Ismail and Roe in [5]. The numerical solutions were executed until they converged to a steady state. We have determined steady state to be at the point where the residuals of all equations have fallen (at least) 5 orders of magnitude from their initial level, as in [8].

To be able to compare the data sets obtained, they need to have the same dimensions. We have used SI-units in our computations. Since the literature on shock density profiles usually presents normalized and non-dimensional profiles, the data used for comparison must be transformed to their dimensional counterparts. The density is normalized by the upstream and downstream densities ρ_1 and ρ_2 (see [2]), such that

$$\rho^* = \frac{\rho - \rho_1}{\rho_2 - \rho_1}. \tag{3.1}$$

The length scale is normalized by the upstream mean free path λ_1, as in [2], where

$$\lambda_1 = \frac{16}{5}\sqrt{\frac{\gamma}{2\pi}}\frac{\mu_1}{\rho_1 c_1}. \tag{3.2}$$

3.1 Numerical Accuracy

Before commencing on the numerical simulations, we must determine the level of resolution needed to ensure sufficient numerical accuracy. The analysis done starts by determining the number of spatial steps needed. The spatial interval is set to be $x \in [-0.01, 0.01]$, based on the interval from the experimental results $x_{\text{exp}} \in [-0.0088, 0.0077]$.

We want to determine the required number of spatial step, such that we can disregard the numerical error of the scheme. We assume this is when two solution computed with a different number of steps are equal. In our analysis, we have compared two solutions where the first one has twice as many steps as the second. When these are equal, the numerical error that comes from the scheme is small enough to not be considered.

We use simulations of the original Navier-Stokes equations computed with Ismail and Roe's entropy-consistent flux as a reference solution. This is used to establish the number of steps needed. These solutions are compared to the solution from Navier-Stokes equations computed with Lax-Friedrichs flux with no artificial diffusion. Since the entropy-consistent scheme has no artificial diffusion, these two schemes should give similar results.

Figure 3.1 shows the density variation in a shock profile for Argon. The two different simulations were done with Ismail-Roe flux (green) and Lax-

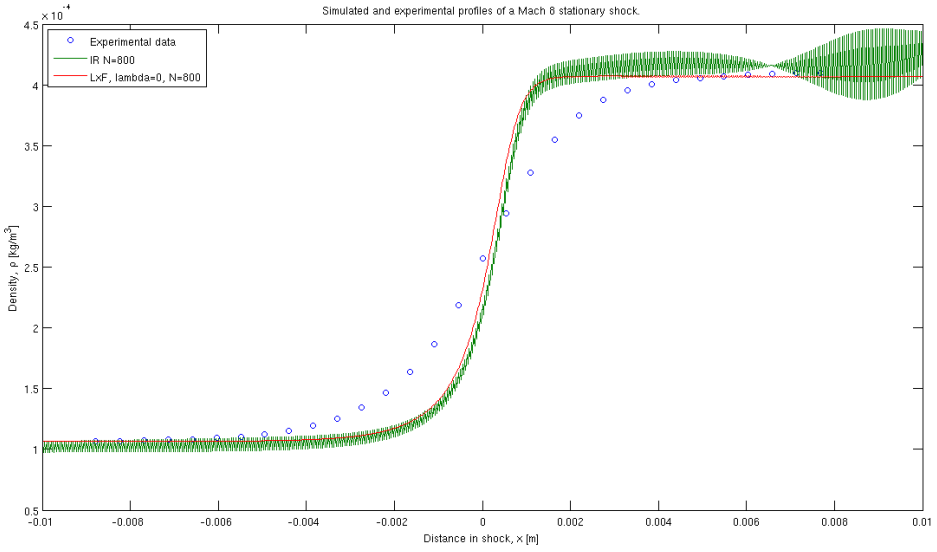

Figure 3.1: Density variation of a shock profile for Argon. The simulations are done with the Navier-Stokes equation. Ismail-Roe's flux is used on the green line, and Lax-Friedrichs flux with no artificial diffusion is used on the red. The dotted blue line represents the experimental data from [2].

Friedrichs flux with no artificial diffusion (red). The grid contained 800 points. We see that these are not similar.

The 400-step case is not shown because of oscillations from the Ismail-Roe flux, which makes the comparison to the 800-step case difficult. However, the difference is clearly reflected in Figure 3.1, and we see that even 800 steps are not enough to reduce the numerical error to a negligible level. In [8], a mesh size of $0.017\lambda_{M1}$ is used, where λ_{M1} is the upstream mean free path. In our case, this would correspond to approximately 11 000 spatial steps. This would be too time consuming, and therefore we will only use 800 steps.

3.2 Diffusion Analysis

The diffusion parameters δ_0, μ_0, μ_1, k_0 and k_1 in equation (1.21) and (1.22) have been varied through the simulations. Tables of the diffusion parameters used are found in Appendix B. Calculations of the parameters used in the simulations are based on the diffusion and heat conductivity coefficients found in [13].

3.2.1 Navier-Stokes parameters

In the first simulation the standard Navier-Stokes equations are computed with $\delta = 0$ and constant μ and k. The mean value of T_1 and T_2, i.e. $T_{\text{mean}} = 3000°$ K, has been used to compute the parameter $\mu = \mu_0$. The relation $\mu = \frac{3k}{4c_p}$, found in [15], has been used to determine $k = k_0$.

Because of the discrete properties of a shock, the simulation was unable to continue after a certain time because of unstable conditions. This has been solved by allowing the shock to acquire some more spatial values, before it was resumed with the Navier-Stokes diffusion parameters. The simulations were done with Brenner-Navier-Stokes constant parameters for the first 200 time steps, where $\delta = k/(\rho c_p)$.

We see a large difference in the simulation where the Ismail-Roe flux has been used, Figure 3.3, and where the Lax-Friedrichs flux, Figure 3.2, is used. The

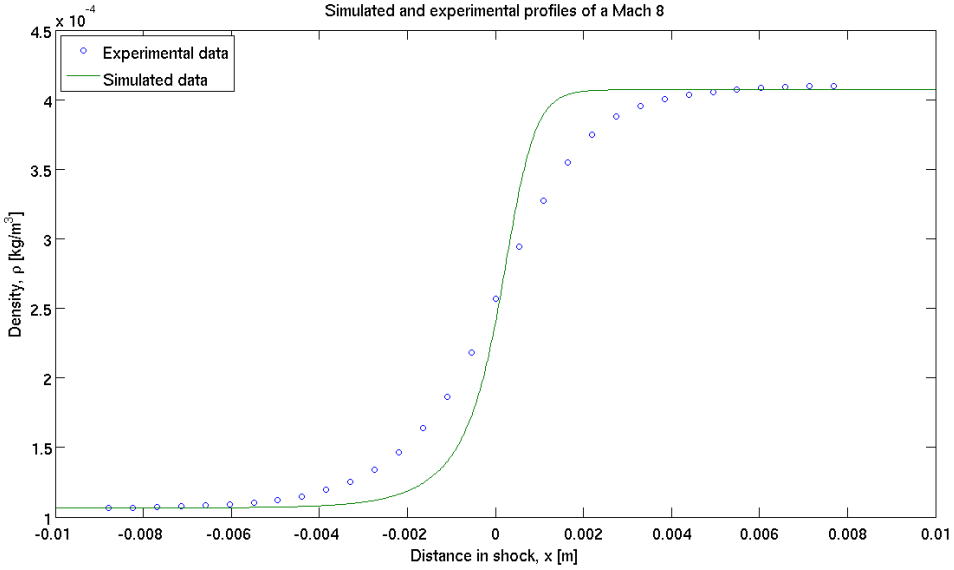

Figure 3.2: Simulated (green) and experimental (blue) density profiles. Computed with the Navier-Stokes equation with Lax-Friedrichs flux.

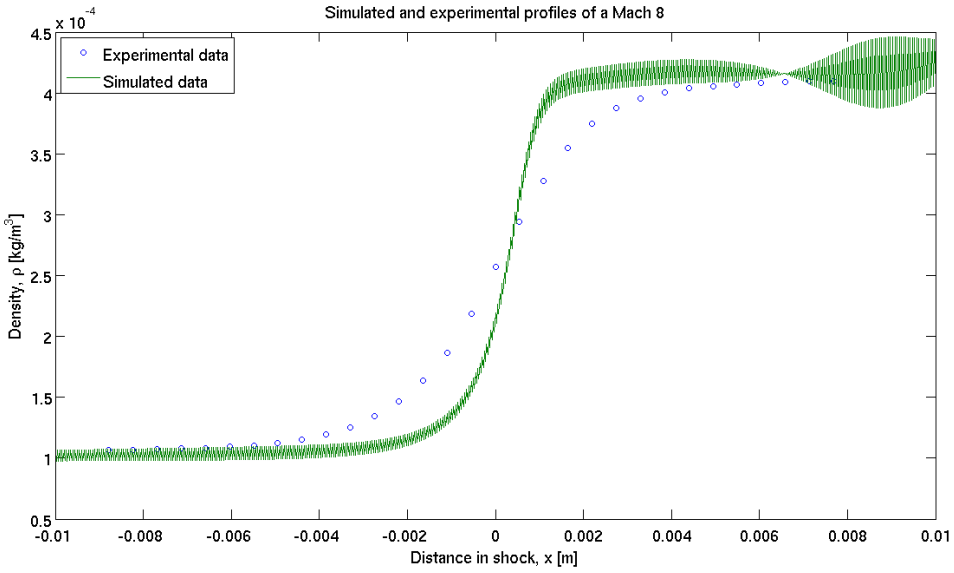

Figure 3.3: Simulated (green) and experimental (blue) density profiles. Computed with the Navier-Stokes equation with Ismail-Roe's flux.

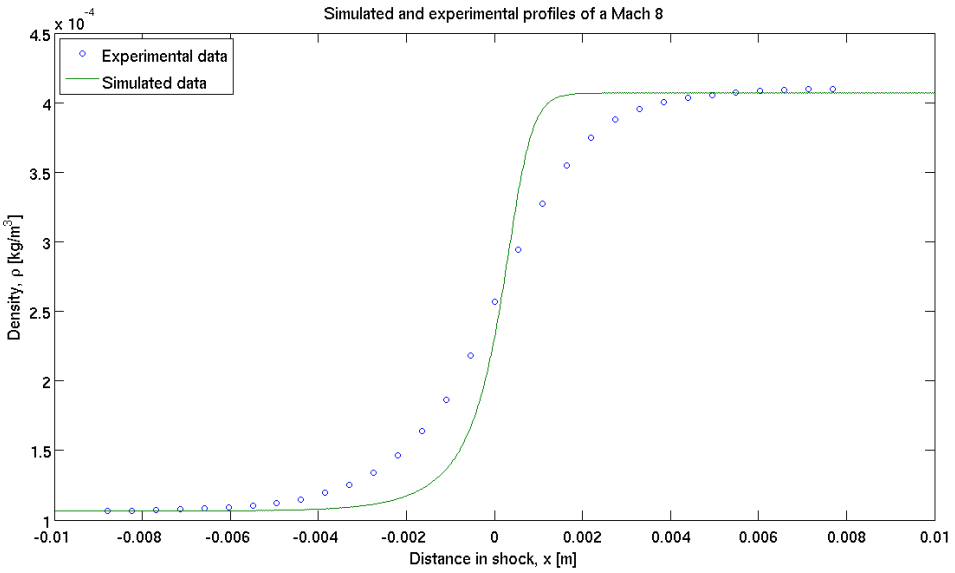

Figure 3.4: Simulated (green) and experimental (blue) density profiles. Computed with the Brenner-Navier-Stokes equation with Ismail-Roe's flux, with very small mass diffusion.

Lax-Friedrichs scheme has artificial viscosity which damps the oscillations produced by the Navier-Stokes equations around the shock.

The oscillations cause instability of the scheme, since it calculates a negative T and ρ. This is physically impossible. The artificial viscosity of the Lax-Friedrichs method may solve this problem, since it damps the oscillations.

It turns out that even though the simulation with Ismail-Roe flux continues to run, the norm of the difference of the numerical solutions at two consecutive time steps does not converge to zero. After it has dropped about five orders of magnitude, convergence stops. After long time, the solution became unstable. This unstable behavior is not unexpected, based on the large oscillates we can see from Figure 3.3.

To investigate the cause of the instability, we computed a simulation with a very small mass diffusion, $\delta = 10^{-5}$. As with the Lax-Friedrichs and

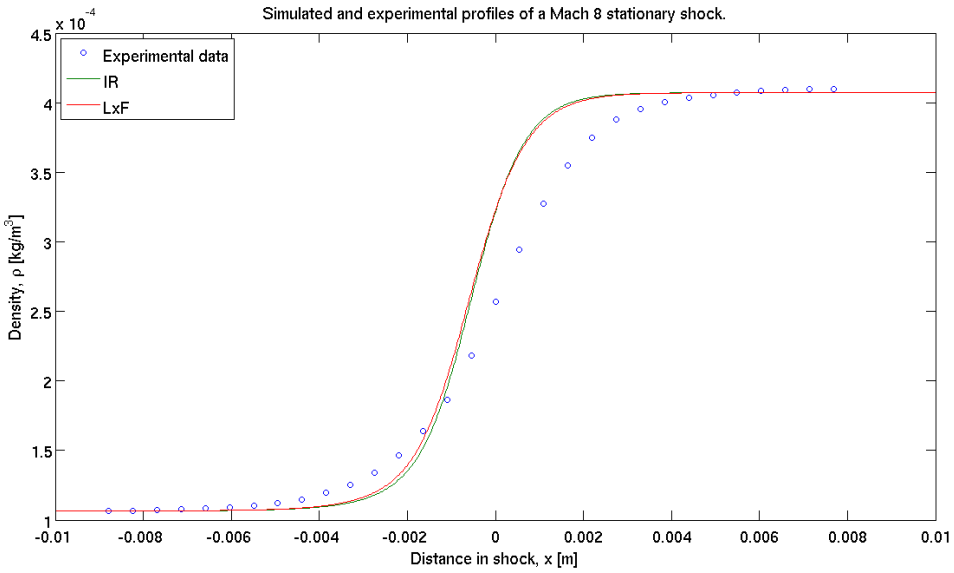

Figure 3.5: Simulated (Ismail-Roe's flux (green) and Lax-Friedrichs flux (red)) and experimental (blue) density profiles, computed with Brenner-Navier-Stokes equation with constant diffusion parameters.

Ismail-Roe case, the shock simulation start with some oscillations. This is only to be expected since we start with a discontinuity. After some initial oscillations, the shock profile stabilizes gradually, and the error continues to converge to zero. The converged solution is depicted in Figure 3.4. Since the Ismail-Roe case is a physically conceivable scheme, this indicates that the positivity problems (negative density and temperature) of the standard Navier-Stokes model is cured with Brenner's model.

3.2.2 Brenner-Navier-Stokes with constant parameters

A simulation of the Brenner-Navier-Stokes system was computed with constant diffusion parameters. μ and k where the same as for the parameters in the Navier-Stokes case, in Section 3.2.1. The relation $\delta = k/(\rho c_p)$ has been used determine δ, where the mean value of ρ_1 and ρ_2 has been used.

As we can see from Figure 3.5, the Brenner-Navier-Stokes equation solves the

shock wave problem more accurate than what the Navier-Stokes equations does. The shock layer thickness predicted by the conventional Navier-Stokes equations is too thin, whereas what the Brenner-Navier-Stokes produce is in better agreement with the experimental data.

However, there seems to be some overshoot. It looks like the simulated values "pass" by and over the experimental values, compared to the previous simulation cases. This may come from too high diffusion parameters. The coefficients μ and k are based on measurements, where they alone constitute the diffusion, whereas in the simulation we have only added the mass diffusion δ, not adjusted for it.

3.2.3 Brenner-Navier-Stokes with variable parameters based on physical measurements

The diffusion parameters μ_0, μ_1, k_0 and k_1 were here found by using a least square method, calculated from tabulated values in [13]. δ was given as in the previous simulation.

As Figure 3.6 shows, there are many similarities between these simulations and the constant-parameter case. Since we here have used variable parameters depending on the temperature T, and there is great differences in the temperature across the shock, these simulations are closer to the experimental data.

The overshoot may again come from too much diffusion.

3.2.4 Brenner-Navier-Stokes with optimized variable parameters

The diffusion parameters found from optimizing the parameters such that the simulation looked as similar to the experimental data as possible, is used in this simulation of the Brenner-Navier-Stokes system. We have used the diffusion parameters from the previous case as a starting point, and tried different alterations to make the simulated solution more similar to the experimental data.

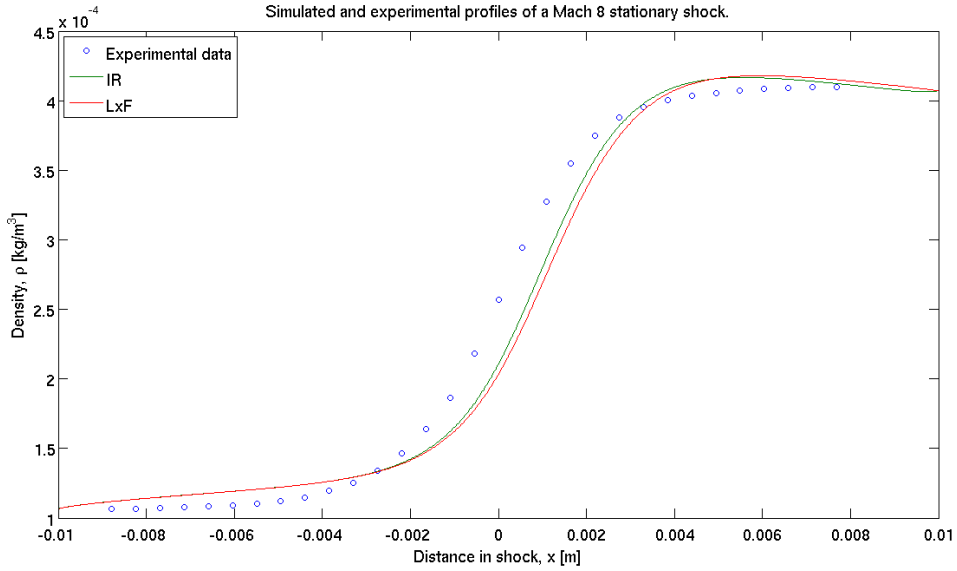

Figure 3.6: Simulated (Ismail-Roe's flux (green) and Lax-Friedrichs flux (red)) and experimental (blue) density profiles, computed with Brenner-Navier-Stokes equation with "physical" diffusion parameters.

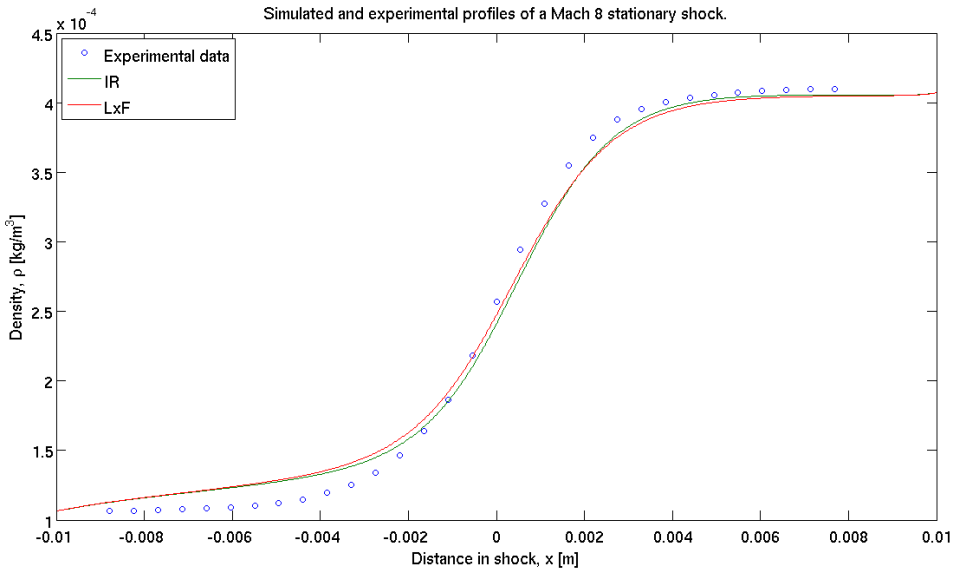

Figure 3.7: Simulated (Ismail-Roe's flux (green) and Lax-Friedrichs flux (red)) and experimental (blue) density profiles, computed with Brenner-Navier-Stokes equation with optimized diffusion parameters (1).

δ was, again, given as in the previous simulations; $\delta = k/(\rho c_p)$, and increased by $\sim 20\%$ for comparison.

There is still an overshot at the shock wave, as we can see in Figure 3.7.

The results for simulations with equal μ and k, and a 20% increased δ, are quite similar, see Figure 3.8. This may indicate that the Brenner-Naver-Stokes equations is a robust model.

3.3 Summary

The results from the simulations are summarized below. The $\mathcal{L}^2$-norm between the exact and simulated solution is given in Table 3.1. The compared data is shown in Figure 3.9 and Figure 3.10, where the results from the Lax-Friedrichs and Ismail-Roe case is given.

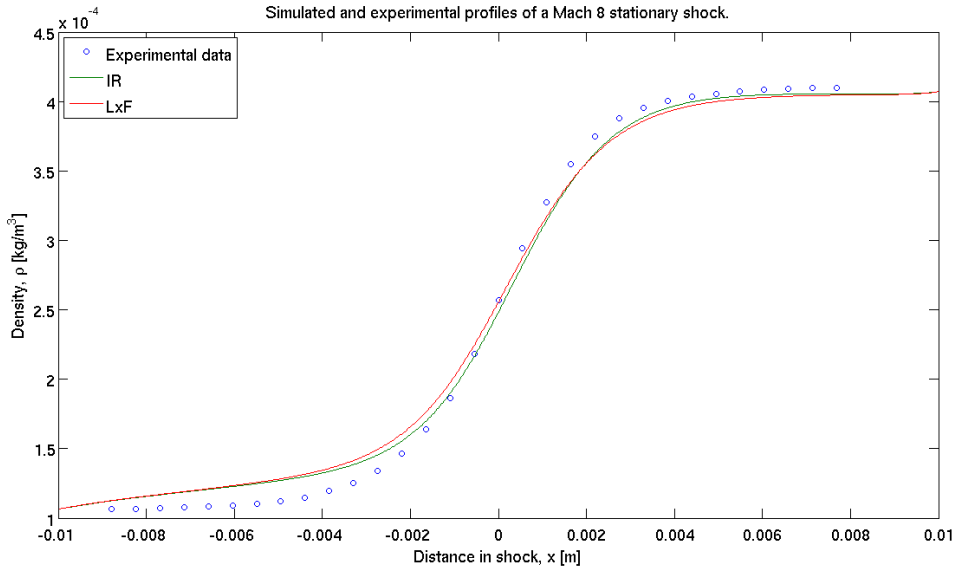

Figure 3.8: Simulated (Ismail-Roe's flux (green) and Lax-Friedrichs flux (red)) and experimental (blue) density profiles, computed with Brenner-Navier-Stokes equation with optimized diffusion parameters (2).

Diffusion model	**Lax-Friedrichs flux**	**Ismail-Roe flux**
Navier-Stokes, constant	$6.46 \cdot 10^{-7}$	$5.91 \cdot 10^{-7}$
Brenner-Navier-Stokes, constant	$6.76 \cdot 10^{-7}$	$6.81 \cdot 10^{-7}$
Brenner-Navier-Stokes, physical	$6.40 \cdot 10^{-7}$	$5.32 \cdot 10^{-7}$
Brenner-Navier-Stokes, optimized (1)	$3.29 \cdot 10^{-7}$	$3.20 \cdot 10^{-7}$
Brenner-Navier-Stokes, optimized (2)	$3.12 \cdot 10^{-7}$	$2.80 \cdot 10^{-7}$

Table 3.1: $L2$-norm of the simulated and experimental results.

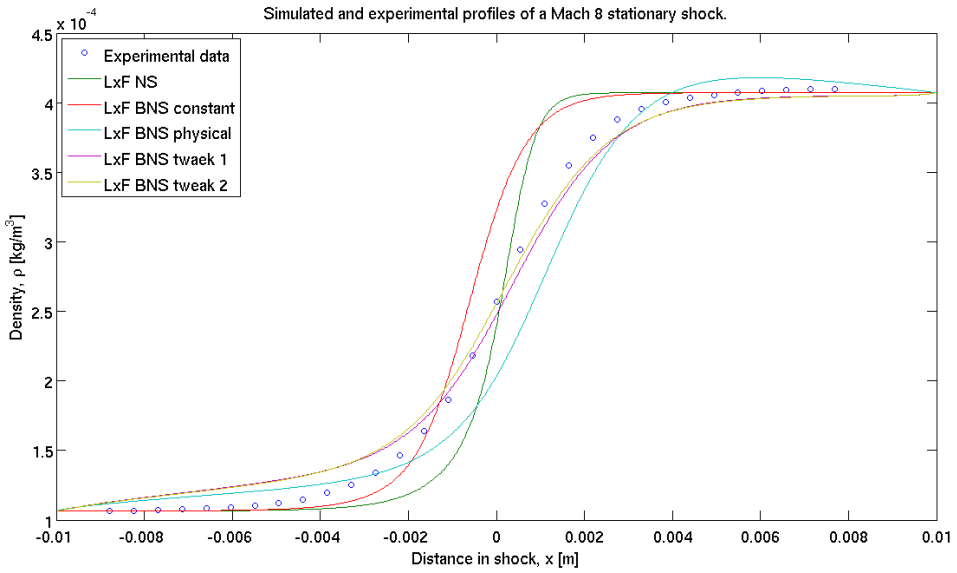

Figure 3.9: Simulated and experimental density profiles, all diffusion models. Computed with Lax-Friedrichs flux.

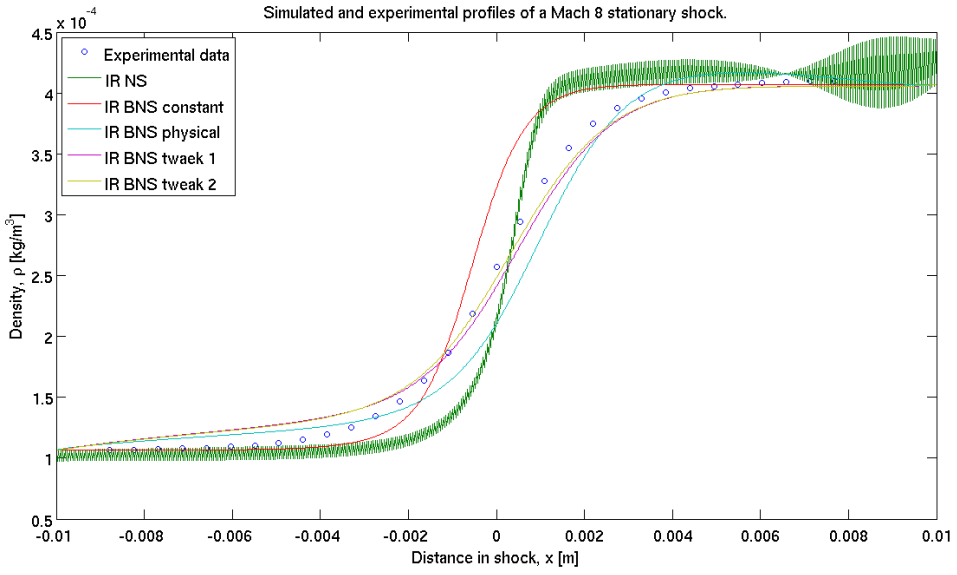

Figure 3.10: Simulated and experimental density profiles, all diffusion models. Computed with Ismail-Roe flux.

Chapter 4

Concluding Remarks and Further Work

In this thesis, the problem presented has been to examine the modified version of the Navier-Stokes system, the Brenner-Navier-Stokes system. This has been reduced to simulations of a shock wave problem in one spatial dimension. Both the original and the modified version of the Navier-Stokes equations has been used to solve the conservation laws (1.5) and (1.18). The simulated solutions, in particular the density ρ, have been compared to experimental measurements of the density of a Mach 8 shock wave in Argon, published in [2].

Even though the Navier-Stokes equations are robust and accurate over a wide range of Knudsen numbers, it seems like the equations are unsuccessful in predicting the correct shock structures for shocks with high Mach numbers.

The new model uses a *known* coefficient for self-diffusion of mass for argon. The simulations done with Brenner's modification to the Navier-Stokes equation does not display an unphysical and unstable behavior.

The model, especially in the Ismail-Roe-flux case, require a small CFL-number to work, and the order of magnitude depends on the size of diffusion parameters. At first it seems as if the program is running properly, but after some time, it explodes and $\mathcal{U}$ is filled with imaginary values. It turns out that

T is computed to be negative, which implies negative density and pressure. This may come from a poor spatial resolution. The natural diffusion of the scheme decreases when Δt increases, such that even though Δx is not changed, the oscillations increases.

Since the Ismail-Roe flux is entropy-consistent, the scheme has no internal diffusion. All the diffusion we see during the simulation, is the physical diffusion.

The mediocre results of the Navier-Stokes simulation with Ismail and Roe's flux, may indicate that mass diffusion need to be added to have a stable and physical reliable simulation.

Brenner's modification improve the predictions of the shock structure, but only with the somewhat arbitrary diffusion coefficient δ based on an upper limit. With a large δ the above equations produce an unphysical behavior. At even higher δ, the simulation becomes unstable. Eventually, a more physically correct model should be derived and adapted for δ, and the other diffusion coefficients.

Even though the convergent solution to the shock wave problem converge to a steady state solution, which by the Lax-Wendroff theorem implies the existence, we have yet to prove that the modified equations admit a weak solution. This would be a natural "next step" in the research process. Further, it would also be interesting with a deeper analysis of why we have positivity problem in cases where simulations goes wrong.

While it is important not to draw strong conclusions based on just one test case, our results are generally encouraging for the Brenner-Navier-Stokes equations. We can clearly see that the this shock profile is much more similar to the experimental data than the Navier-Stokes profile is. It seems only to be the more detailed features of the shock profile that Brenner's models do not reproduce as well. However, these inaccuracies may come from using too large diffusion coefficients.

Bibliography

[1] Feireisl E. and Vasseur A. New Perspective in Fluid Dynamics: Mathematical Analysis of a Model Proposed by Howard Brenner. *Advances in Mathematical Fluid Mechanics*, 2009.

[2] Steinhilper E. *Electron beam measurements of the shock wave structure.* PhD thesis, California Institute of Technology, 1971.

[3] Tadmor E. Entropy stable approximations of Navier-Stokes equations with no artificial numerical viscosity. *Journal of Hyperbolic Differential Equations*, Vol 3:529–559, 2006.

[4] Tadmor E. and Shong W. Entropy stability theory for difference approximations of nonlinear conservation laws and related time-dependent problems. *Acta Numerica*, Vol 2003:451–512, 2003.

[5] Ismail F. and Roe P. Affordable, entropy-consistent Euler flux functions II: Entropy production at shocks. *Journal of Computational Physics*, Vol 228:5410–5436, 2009.

[6] Alsmeyer H. Density profiles in argon and nitrogen shock vanes measured by absorption of an electron beam. *Journal of Fluid Mechanics*, Vol 74:497–513, 1976.

[7] Greenshields C. J. and Reese J. M. The structure of hypersonic shock waves using Navier-Stokes equations modified to inculde diffusion. *http://arxiv.org/abs/0706.0141v1 [physics.flu-dyn]*, 2007.

[8] Greenshields C. J. and Reese J. M. The structure of shock waves as a test of Brenner's modification to the Navier-Stokes equations. *Journal of Fluid Mechanics*, Vol 580:407–429, 2007.

[9] LeVeque R. J. *Numerical Methods for Conservation Laws.* Birkhauser Verlag, 1992.

[10] Svärd M. Lecture notes in Numerical Partial Differential Equations. University of Edinburgh, 2011.

[11] Temam R. M. and Miranville A. M. *Mathematical Modeling in Continuum Mechanics.* Cambridge, 2005.

[12] Kundu P., Cohen I., and Dowling D. *Fuid Mechanics.* Academic Press, 5th edition, 2012.

[13] Lide D. R. *Handbook of Chemistry and Physics.* Taylor & Francis Group, 2009.

[14] Gottlieb S., Shu C., and Tadmor E. Strong Stability-Preserving Hgh-Order Time Discretization Methods. *SIAM Review*, Vol 43:89–112, 2001.

[15] Čermý R. and Vodák F. A theoretical relation between ciscosity and thermal conductivity of gases based on macroscopic balance equations. *Czechoslovak Journal of Physics*, Vol 44:913–926, 1994.

Appendix A

The Ismail-Roe entropy-stable flux for the Euler equations

The Ismail-Roe entropy-stable flux for the Euler equations used in the simulations is given under. This is found in [5]. The reader is referred to [4] and [5] for a deeper analysis. The variable H is used for the total enthalpy.

An entropy-stable flux for the Euler equation is

$$\mathbf{f}^* = \mathbf{f}_c - \frac{1}{2}\hat{\mathbf{R}}\hat{\mathbf{D}}\hat{\mathbf{R}}^T[\mathbf{v}], \tag{A.1}$$

where $\mathbf{f}_c$ is the entropy-conservative flux (see under), $\hat{\mathbf{R}}$ contains the averaged right eigenvectors of $\mathbf{A}$

$$\hat{\mathbf{R}} = \begin{bmatrix} 1 & 1 & 1 \\ \hat{\mathcal{U}} - \hat{u} & \hat{\mathcal{U}} & \hat{\mathcal{U}} - \hat{u} \\ \hat{H} - \hat{\mathcal{U}}\hat{u} & \frac{1}{2}\hat{\mathcal{U}}^2 & \hat{H} + \hat{\mathcal{U}}\hat{u} \end{bmatrix}. \tag{A.2}$$

$\hat{\mathbf{D}}$ is the positive dissipation matrix that is written as

$$\hat{\mathbf{D}} = \left(\hat{\boldsymbol{\lambda}} + \frac{1}{6}|[\boldsymbol{\lambda}_{\mathcal{U}\pm u}]|\right)\hat{\mathbf{S}}, \tag{A.3}$$

where $\hat{\boldsymbol{\lambda}}$ is the matrix of absolute eigenvalues

$$\hat{\boldsymbol{\lambda}} = \text{diag}(|\hat{\mathcal{U}} - \hat{u}|, |\hat{\mathcal{U}}|, |\hat{\mathcal{U}} + \hat{u}|). \tag{A.4}$$

$[\boldsymbol{\lambda}_{\mathcal{U}\pm u}]$ = adds extra dissipation only to acoustic waves

$$[\boldsymbol{\lambda}_{\mathcal{U}\pm u}] = \text{diag}(|\hat{\mathcal{U}} - \hat{u}|, 0, |\hat{\mathcal{U}} + \hat{u}|), \tag{A.5}$$

and $\hat{\mathbf{S}}$ is a matrix that produces the correct scaling

$$\hat{\mathbf{S}} = \text{diag}\left(\frac{\hat{\rho}}{2\gamma}, \frac{(\gamma-1)\hat{\rho}}{\gamma}, \frac{\hat{\rho}}{2\gamma}\right) \tag{A.6}$$

such that $\mathbf{R}^{-1}d\mathcal{U} = \mathbf{S}\mathbf{R}^T d\mathbf{v}$. The averaged $(\hat{\cdot})$ values for the asymmetric flux ($\hat{\mathbf{R}}\hat{\mathbf{D}}\hat{\mathbf{R}}^T[\mathbf{v}]$) are determined exactly as the averaged values for $\mathbf{f}_c$.

The **entropy conserving flux** satisfies

$$\mathbf{v^T f_c} = [\rho\mathcal{U}], \tag{A.7}$$

and is explicitly computed as averaged quantities of

$$\mathbf{f}_c(\mathcal{U}_L, \mathcal{U}_R) = \begin{bmatrix} \hat{\rho}\hat{\mathcal{U}} \\ \hat{\rho}\hat{\mathcal{U}}^2 + \hat{p}_1 \\ \hat{\rho}\hat{\mathcal{U}}\hat{H} \end{bmatrix}. \tag{A.8}$$

We now determine these averaged states. Define

$$z_1 = \sqrt{\frac{\rho}{p}}, \quad z_2 = \sqrt{\frac{\rho}{p}}\mathcal{U}, \quad z_3 = \sqrt{\rho p}, \tag{A.9}$$

so that the averaged quantities are computed as functions of arithmetic mean $\bar{u} = \frac{u_L + u_R}{2}$ and the logarithmic mean (as defined below). We choose $\hat{\mathcal{U}} = \frac{\bar{z}_2}{\bar{z}_1}$ and insert it into equation (A.1) to obtain

$$\hat{\rho} = \bar{z}_1 \bar{z}_3^{\ln}, \tag{A.10}$$

$$\hat{p}_1 = \frac{\bar{z}_3}{\bar{z}_1}, \tag{A.11}$$

$$\hat{p}_2 = \frac{\gamma+1}{2\gamma}\frac{\bar{z}_3^{\ln}}{\bar{z}_1^{\ln}} + \frac{\gamma-1}{2\gamma}\frac{\bar{z}_3}{\bar{z}_1}, \tag{A.12}$$

$$\hat{u} = \left(\frac{\gamma\hat{p}_2}{\hat{\rho}}\right)^{\frac{1}{2}}, \tag{A.13}$$

$$\hat{H} = \frac{\hat{u}^2}{\gamma-1} + \frac{\hat{\mathcal{U}}^2}{2}. \tag{A.14}$$

Let a be some quantity of interest which has a left and right state. The **logarithmic mean** of a is defined as

$$a^{\ln}(L,R) = \frac{a_L - a_R}{\ln(a_L) - \ln(a_R)}. \tag{A.15}$$

However, this is not numerically well-posed when $(a_L) \to (a_R)$. To overcome this, we write the logarithmic mean on another form. Let $\zeta = \frac{a_L}{a_R}$ so that

$$a^{\ln}(L,R) = \frac{a_L + a_R}{\ln\zeta}\frac{\zeta - 1}{\zeta + 1}, \tag{A.16}$$

where

$$\ln(\zeta) = 2\left(\frac{1-\zeta}{1+\zeta} + \frac{1}{3}\frac{(1-\zeta)^3}{(1+\zeta)^3} + \frac{1}{5}\frac{(1-\zeta)^5}{(1+\zeta)^5} + \frac{1}{7}\frac{(1-\zeta)^7}{(1+\zeta)^7} + O(\zeta^9)\right) \tag{A.17}$$

to obtain a numerically well-formed logarithmic mean. The subroutine for computing the logarithmic mean is the following; let

$$\zeta = \frac{a_L}{a_R}, \quad f = \frac{\zeta - 1}{\zeta + 1}, \quad \mathcal{U} = f * f.$$

1. if($\mathcal{U} < \epsilon$)
   $$F = 1.0 + \mathcal{U}/3.0 + \mathcal{U} * \mathcal{U}/5.0 + \mathcal{U} * \mathcal{U} * \mathcal{U}/7.0$$
2. else
   $$F = \ln(\zeta)/2.0/(f)$$

so that $a^{\ln}(L,R) = \frac{a_L + a_R}{2F}$ with $\epsilon = 10^{-2}$.

Appendix B

Experimental data and physical parameters

B.1 Thermodynamic properties, [6]

λ_1	=	1.098 mm
T_1	=	300° K
p_1	=	50 mTorr
c_p	=	532
γ	=	5/3
R	=	208.5

Table B.1: Thermodynamic properties from NBS Circular (1995)

B.2 Experimental denisty values, [2]

x/λ_1	density ρ^*
−8.0	0.001
−7.5	0.001
−7.0	0.002
−6.5	0.004

−6.0	0.006
−5.5	0.009
−5.0	0.013
−4.5	0.019
−4.0	0.028
−3.5	0.043
−3.0	0.062
−2.5	0.092
−2.0	0.133
−1.5	0.190
−1.0	0.266
−0.5	0.372
0.0	0.500
0.5	0.624
1.0	0.735
1.5	0.826
2.0	0.892
2.5	0.936
3.0	0.962
3.5	0.977
4.0	0.989
4.5	0.995
5.0	1.000
5.5	1.004
6.0	1.006
6.5	1.008
7.0	1.009

Table B.2: Experimentally determined shock wave density profile for a Mach 8 shock in argon

B.3 Diffusion parameters

δ_0	0
μ_0	$11.5 \cdot 10^{-5}$
μ_1	0
k_0	$8.4 \cdot 10^{-2}$
k_1	0

Table B.3: Navier-Stokes diffusion parameters

δ_0	0.611
μ_0	$11.5 \cdot 10^{-5}$
μ_1	0
k_0	$8.4 \cdot 10^{-2}$
k_1	0

Table B.4: Brenner-Navier-Stokes diffusion parameters, constant diffusion parameters

δ_0	0.611
μ_0	$-2.8 \cdot 10^{-5}$
μ_1	$2.7 \cdot 10^{-6}$
k_0	$9.5 \cdot 10^{-3}$
k_1	$6.5 \cdot 10^{-8}$

Table B.5: Brenner-Navier-Stokes diffusion parameters, physical variable diffusion parameters

δ_0	0.611
μ_0	$-2.8 \cdot 10^{-5}$
μ_1	$2.7 \cdot 10^{-6}$
k_0	$1.8 \cdot 10^{-2}$
k_1	$3.5 \cdot 10^{-8}$

Table B.6: Brenner-Navier-Stokes diffusion parameters, optimized variable diffusion parameters 1

δ_0	0.75
μ_0	$-2.8 \cdot 10^{-5}$
μ_1	$2.7 \cdot 10^{-6}$
k_0	$1.8 \cdot 10^{-2}$
k_1	$3.5 \cdot 10^{-8}$

Table B.7: Brenner-Navier-Stokes diffusion parameters, optimized variable diffusion parameters 2